Photoinduced tautomeric transformations of xanthurenic acid†

Vadim V. Yanshole,[a] Peter S. Sherin,[a] Nina P. Gritsan,[b] Olga A. Snytnikova,[a] Victor I. Mamatyuk,[c] Jakob Grilj,[d] Eric Vauthey,[d] Renad Z. Sagdeev[a] and Yuri P. Tsentalovich*[a]

Received 12th January 2010, Accepted 12th May 2010
DOI: 10.1039/c000735h

The properties of xanthurenic acid (XAN) in ground and photoexcited states have been studied using steady-state and time-resolved optical methods as well as quantum chemistry calculations. In neutral aqueous solution and in alcohols, XAN is present in a single tautomeric form (keto form), whereas in aprotic solvents and probably in basic aqueous solutions, more than one tautomeric form is present. UV irradiation of aqueous and alcoholic solutions of XAN results in a very rapid solvent-assisted tautomerization to the enol form, the later undergoes solvent-assisted transformation back to the keto form. The photolysis of XAN in aprotic solvents gives rise to the formation of numerous intermediate forms of XAN in both triplet and ground states. Under intense laser irradiation, XAN undergoes biphotonic ionization, the precursor for ionization being the excited singlet state.

Introduction

The primate lens contains a group of low-molecular weight compounds that absorb UV light in the 300–400 nm spectral range. These compounds—kynurenine (KN) and its derivatives—protect the retina and the lens from UV-induced damage.[1–3] They are chemically and photochemically stable: under physiological conditions, the lifetime of kynurenine can be estimated as several weeks,[4,5] and the quantum yield of kynurenine photodecomposition[5,6] is $1–2 \times 10^{-5}$. Nevertheless, photochemical, thermal, and enzymatic reactions of kynurenine and its derivatives can produce reactive species, which are able to interact with the lens proteins causing modifications. It was proposed that such reactions may give an important contribution to age-related nuclear cataract development.[7–13] In particular, UV irradiation of KN aqueous solutions results in the formation of the triplet state ^{T}KN with a yield of about 2%,[14] which can undergo an electron transfer reaction with amino acid residues of proteins;[13,15] spontaneous deamination of KN and its derivatives affords highly reactive carboxyketoalkenes,[4,5,16] which can bind to the nucleophylic residues of proteins[17–22] (cysteine, lysine, and histidine), disrupting protein functionality and increasing their susceptibility to UV light.[6,12,23]

The reactions of UV filters can also produce hydroxyquinolines. It has been shown[5] that 4-hydroxyquinoline (4HQN) is one of the final products of KN thermal and/or photochemical decomposition under physiological conditions (neutral aqueous solution, $T = 37$ °C). 4,8-Dihydroxyquinoline-2-carboxylic acid (xanthurenic acid, XAN) can be formed from 3-hydroxykynurenine either through spontaneous deamination followed by cyclization, or under the action of an enzyme kynurenine aminotransferase.[24–26] The presence of XAN and its glucoside in cataractous human lenses was reported;[25,27,28] however, XAN has not been found in normal lenses.[29] The absence of this compound in normal lenses may indicate that it is chemically or photochemically much more active than KN and its derivatives, and, once produced, undergoes thermal or photochemical reactions, so that its concentration in the lens remains below detectable levels. The goal of the present work is to study the spectroscopic properties and the photoinduced reactions of XAN and to determine whether this compound can play a role of chromophore for cataractogenesis.

Depending on the solvent nature, hydroxyquinolines can exist in different tautomeric forms, and also undergo protonation and deprotonation. Scheme 1 shows the tautomeric forms of XAN which can exist under acidic, neutral and basic conditions. It has been reported[25] that in alkaline and in 90% ethanol solutions xanthurenic acid is present in two forms, namely enol XAN_e and diketo XAN_{dk} (Scheme 1), and that the fluorescence of XAN_{dk} is much stronger than that of XAN_e. It was also noticed[25] that XAN_{dk} is readily oxidized at room temperature forming di-oxo-xanthurenic acid (DOXA), which has even stronger fluorescence than XAN_{dk}. Optical excitation of hydroxyquinolines can cause an alteration of acidity of protropic functional groups and a shift in the tautomeric equilibrium,[30–33] which leads to numerous solvent-assisted isomerization reactions. Therefore, for a better understanding of XAN photochemistry it is important to determine the energetically favorable forms of this compound in the ground and photoexcited states in different solvents.

Photochemical studies of XAN were performed by Roberts *et al.*[34] It has been revealed that XAN dissolved in CD_3OD

[a] *International Tomography Center SB RAS, Institutskaya str. 3a, 630090 Novosibirsk, Russia*
[b] *Institute of Chemical Kinetics and Combustion SB RAS, Institutskaya str. 3, 630090 Novosibirsk, Russia*
[c] *Novosibirsk Institute of Organic Chemistry, Acad. Lavrentjev av. 9, 630090 Novosibirsk, Russia*
[d] *Department of Physical Chemistry, University of Geneva, 30 quai Ernest-Ansermet, CH-1211 Geneva 4, Switzerland*

† Electronic supplementary information (ESI) available: TA time profiles measured in XAN basic solution photolysis in the presence and absence of acetone; the dependence of TA intensity on the laser energy. See DOI: 10.1039/c000735h

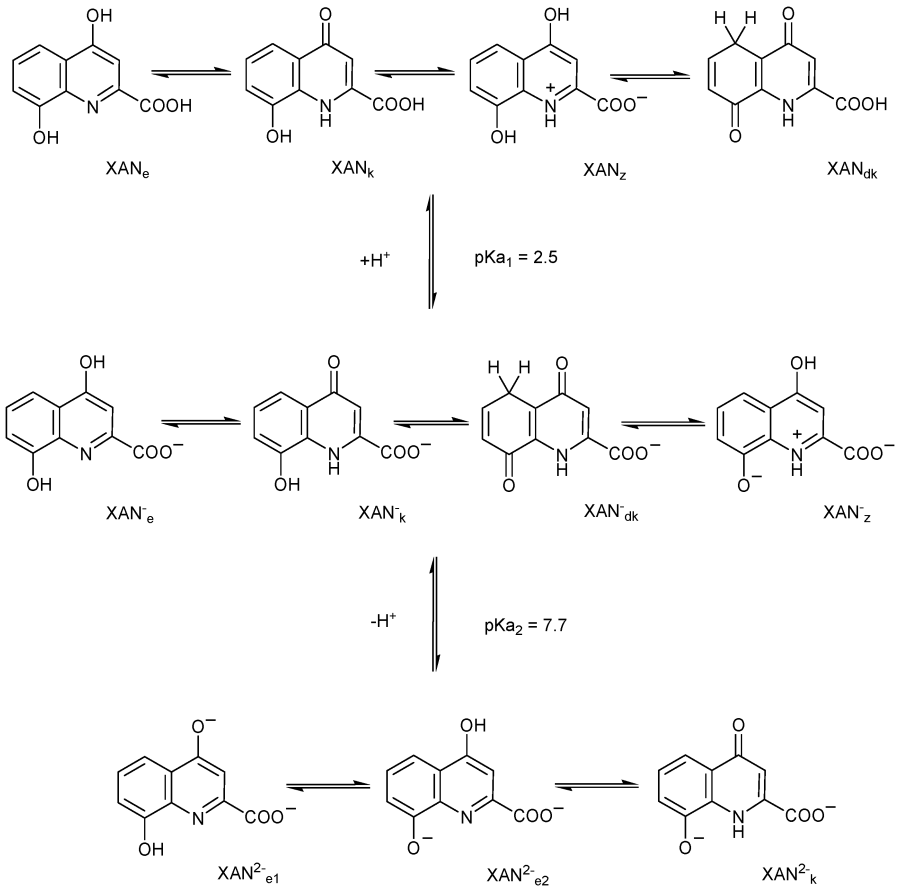

Scheme 1

produces singlet oxygen with a quantum yield of $\phi_\Delta = 0.17$, which is much higher than the singlet oxygen yields for UV filters: for example, for KN $\phi_\Delta = 0.006$;[34] for another UV filter, 3-hydroxykynurenine, the value of ϕ_Δ was reported to be below detectable level.[35] Theoretical calculations[36] demonstrate that the energy of the T_1 level of XAN (2.6 eV) is sufficient to generate both singlet oxygen $^1O_2$ and superoxide $O_2^{\bullet -}$. Irradiation of lens crystallins in the presence of XAN results in protein oxidation and polymerization.[26,37] In the present study, we applied a combination of experimental methods and quantum chemical calculations to clarify the properties of XAN in the ground and excited states and the mechanisms of XAN photochemical reactions in different solvents.

Experimental

Materials

4,8-Dihydroxyquinoline-2-carboxylic acid (XAN) was used as received from Sigma/Aldrich. H_2O was doubly distilled. The organic solvents acetone, methanol (MeOH), ethanol (EtOH), *N*,*N*-dimethylformamide (DMF) and dimethylsulfoxide (DMSO) as well as the deuterated solvents D_2O and DMSO-d_6 from Sigma/Aldrich were used as received.

NMR and steady-state optical measurements

The NMR spectra were obtained with the use of a NMR spectrometer AV-400 (Bruker Biospin). UV-visible electronic absorption spectra were recorded with an Agilent 8453 UV-visible spectrometer. Fluorescence emission and excitation spectra were measured with a Cary Eclipse fluorimeter (Varian). All samples were deoxygenated by argon bubbling for 15 min prior to measurements, capped, and sealed with parafilm. The fluorescence emission and excitation spectra were corrected for the wavelength dependence of the spectrometer's detection. The response of the pure solvent has been subtracted from all spectra reported here and the contribution of Rayleigh and Raman scattering should therefore be minimized. Fluorescence quantum yields were determined by comparison with that of quinine sulfate in 0.1 M H_2SO_4 ($\Phi = 0.577$).[38]

Nanosecond laser flash photolysis (LFP)

A detailed description of the LFP equipment has been published earlier.[39,40] The sample solutions, placed in a rectangular cell (inner dimensions 10 mm × 10 mm), were irradiated with a Quanta-Ray LAB-130-10 Nd:YAG laser (pulse duration 8 ns; 355 nm, pulse energy up to 150 mJ; 266 nm, pulse energy up to 70 mJ). The dimensions of the laser beam at the front of the cell were 3 mm × 8 mm. The monitoring system includes a DKSh-150 xenon short-arc lamp connected to a high current pulser, a home-made monochromator, a 9794B photomultiplier (Electron Tubes Ltd.), and a LeCroy 9310A digitizer. The monitoring light, concentrated in a rectangle of 2.5 mm height and 1 mm width, passed through the cell along the front (laser irradiated) window. Thus, in all experiments the excitation

optical length was 1 mm, and the monitoring optical length was 8 mm. All solutions were bubbled with argon or oxygen for 15 min prior to, and during, irradiation.

Femtosecond pump–probe transient absorption measurements

The experimental setup for pump–probe transient absorption (TA) measurements has been described in detail elsewhere.[41] Excitation was performed at 400 nm using the frequency-doubled output of a standard 1 kHz amplified Ti:Sapphire system (Spectra-Physics). The pump intensity on the sample was around 3 μJ. Probing was achieved with a white-light continuum obtained by focusing a small fraction of the 800 nm pulses in a CaF_2 plane window. The polarization of the probe pulses was at the magic angle relative to that of the pump pulses. All spectra were corrected for the chirp of the white light probe pulses. The FWHM of the instrument response function was *ca.* 200 fs. The sample solutions were placed in a 1 mm thick quartz cell where they were continuously stirred by N_2-bubbling. Their absorbance at the excitation wavelength was around 0.15.

Time-resolved fluorescence measurements

The early fluorescence dynamics were measured using the fluorescence upconversion setup described in detail elsewhere.[42] Briefly, part of the output of a mode locked Ti:sapphire laser (Spectra Physics "Mai Tai") was frequency doubled and used to excite the sample at 370 nm. The fluorescence was gated by sum-frequency mixing with the fundamental of the laser output. The up-converted UV photons were directed into a monochromator and detected by a photomultiplier with photon counting electronics. The sample solutions were kept in a 1.0 mm thick spinning cell. The full width at half maximum (FWHM) of the instrument response function was around 210 fs.

Quantum chemical calculations

The geometries of keto and enol forms, protonated and deprotonated, triplet excited state and cation and anion radicals of XAN were optimized at the B3LYP/6-31G(d) level.[43,44] Previously[45] we demonstrated that this method performs well for the calculations of the thermodynamics of 4-hydroxyquinoline transformations. All equilibrium structures were ascertained to be minima on the potential energy surfaces. All calculations were performed with the Gaussian-03 suite of programs.[46] The influence of the solvent (water and DMSO) on the free energies of formation was taken into account using the PCM model[47] as implemented to Gaussian-03.

Results and discussion

1 Properties of the XAN ground state

1.1 Steady state optical absorption spectra. Fig. 1a shows the electronic absorption spectra of XAN obtained in aqueous acidic, neutral, and basic solutions, and reveals that this compound has more than one protonation site (Scheme 1). The pH dependence of the optical absorption of XAN solution (insert in Fig. 1a) was measured at 255 nm, where the difference between the absorption of the protonation forms is most pronounced. Simulation of the titration curve gives the values of the dissociation constants pK_{a1} = 2.5 and pK_{a2} = 7.7. Most probably, the value pK_{a1} = 2.5, typical for many weak acids, corresponds to the protonation of the carboxyl group. However, our recent studies of the related compound, 4-hydroxyquinoline (4HQN), demonstrated[45] that the pK_a value of the amino group in 4HQN is 2.4. Moreover, unsatisfactory agreement between the experimental and calculated titration curves in the acidic region probably means that both the carboxyl group and the nitrogen atom can undergo protonation in the pH 0.5–2.5 region. Theoretical calculations (Table 1) predict that in aqueous acidic solutions, all four possible structures are rather close in energy, and that the keto XAN_k and zwitterionic XAN_z structures are energetically most favorable. At the same time, calculations performed for the anion XAN^- demonstrate that the free energy of the keto form XAN^-_k in aqueous neutral (or moderately acidic) solution is significantly lower than the free energies of the enol XAN^-_e, diketo XAN^-_{dk}, and zwitterionic XAN^-_z forms (Table 1).

The assignment of the second dissociation constant pK_{a2} = 7.7 is not obvious. As shown in Scheme 1, three different tautomeric forms (XAN^{2-}_{e1}, XAN^{2-}_{e2}, and XAN^{2-}_k) can exist at high pH. The XAN^{2-}_{e1} and XAN^{2-}_k forms seem to be more favorable, since intramolecular hydrogen bonds between nitrogen and hydroxyl group should act as an

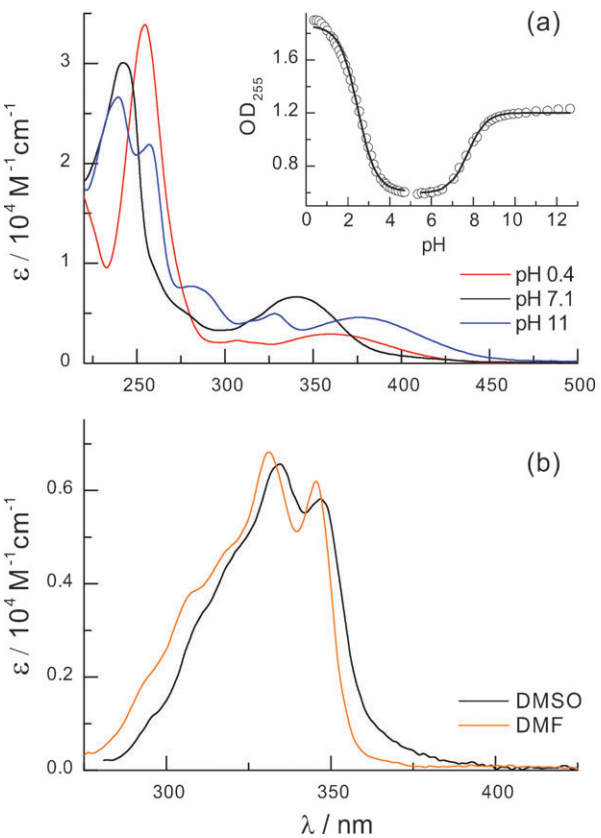

Fig. 1 (a) UV-visible absorption spectra of XAN aqueous solutions at different pH. Insert: pH dependence of the solution optical density at 255 nm. (b) UV-visible absorption spectra of XAN in DMSO and DMF.

Table 1 Relative Gibbs free energies of different forms of XAN predicted by the B3LYP/6-31G(d) calculations in the gas phase and in solution using the PCM model. Energetically most favorable forms are indicated by bold font

Neutral form (XAN)				
	XAN_e	XAN_k	XAN_{dk}	XAN_z
$\Delta(\Delta G)$ (gas phase)	**0**	3.1 kcal mol^{-1}	4.2 kcal mol^{-1}	16.1 kcal mol^{-1}
$\Delta(\Delta G)$ (DMSO)	**0**	**0.1 kcal mol^{-1}**	2.5 kcal mol^{-1}	3.0 kcal mol^{-1}
$\Delta(\Delta G)$ (H_2O)	0	**−1.8 kcal mol^{-1}**	1.2 kcal mol^{-1}	**−1.4 kcal mol^{-1}**
Anion (XAN^-)				
	XAN^-_e	XAN^-_k	XAN^-_{dk}	XAN^-_z
$\Delta(\Delta G)$ (gas phase)	0	**−13.2 kcal mol^{-1}**	−9.9 kcal mol^{-1}	−6.5 kcal mol^{-1}
$\Delta(\Delta G)$ (H_2O)	0	**−8.7 kcal mol^{-1}**	−2.1 kcal mol^{-1}	−0.1 kcal mol^{-1}
Dianion (XAN^{2-})				
	XAN^{2-}_{e1}	XAN^{2-}_{e2}	XAN^{2-}_k	
$\Delta(\Delta G)$ (gas phase)	0	19.5 kcal mol^{-1}	**−16.4 kcal mol^{-1}**	
$\Delta(\Delta G)$ (H_2O)	**0**	8.8 kcal mol^{-1}	**−1.9 kcal mol^{-1}**	

additional stabilizing factor. This assumption is confirmed by the results of DFT calculations (Table 1): the free energies of these forms are much lower than that of XAN^{2-}_{e2}.

The absorption spectra of XAN were also recorded in the non-aqueous polar solvents methanol, ethanol, DMF and DMSO. It has been previously reported that XAN is insoluble in alcohols.[48] However, we found that, even in dry MeOH, the solubility of XAN at room temperature is above 10^{-3} M. The spectra obtained in both alcoholic solutions (not shown) are similar to each other and to the spectrum obtained in aqueous neutral solution; the spectra recorded in aprotic solvents DMF and DMSO (Fig. 1b) are similar to each other, but differ significantly from the spectra obtained in protic solvents.

1.2 Fluorescence spectra and quantum yields. The intensity of XAN fluorescence is strongly solvent dependent. Table 2 gives the data on the total fluorescence quantum yields Φ_{fl} measured in different solvents upon excitation at 280, 300, 330 and 360 nm. In protic solvents, there is an obvious correlation between the Φ_{fl} value and the hydrogen-bonding ability of the solvent: the fluorescence is weaker in more protic solvents. This result testifies that hydrogen bonding plays an important role in the deactivation of photoexcited XAN. As a reference, the values of Kamlet–Taft's solvatochromic parameter α,[49,50] characterizing the hydrogen-bonding ability of the solvent, are presented in Table 2.

The fluorescence emission and excitation spectra of XAN were recorded in methanol, ethanol, DMF, and acidic, neutral and basic aqueous solutions. In alcohols, the excitation spectra are very similar to the absorption spectra obtained in the same solvent, and the emission spectra only slightly change with the variation of the excitation wavelength. As an example, the fluorescence spectra of XAN in ethanol are shown in Fig. 2c. The obtained results testify that in methanol and in ethanol only one fluorescent tautomeric form of XAN is present.

In aqueous solutions, the dependence of the emission spectra on the excitation wavelength is more significant (Fig. 2a and b). One should notice that XAN fluorescence in aqueous solutions is very weak (Table 2), and even minor amounts of fluorescent impurities or fluorescent tautomeric forms can significantly distort the spectral shape. It is noteworthy nevertheless that the most pronounced changes in emission spectra with the variation of the excitation wavelength occur in basic solutions, where the fluorescence is the strongest. Basic solutions are also characterized by a significant dependence of the fluorescence quantum yield on the excitation wavelength (Table 2), which points to the presence of more than one tautomeric forms of XAN in basic solutions.

The fluorescence excitation spectra in DMF (Fig. 2d) differ significantly from the absorption spectra and exhibit a dependence on the detection wavelength; the fluorescence emission spectra and the fluorescence quantum yield depend on the excitation wavelength. Thus, the fluorescence data indicate that in DMF, and probably in basic aqueous solutions, XAN is present in more than one tautomeric form. Since the fluorescence properties of the individual tautomeric forms of XAN are unknown, it is difficult to estimate from our data the relative amounts of the different XAN forms in these solutions.

1.3 NMR data. Fig. 3a shows the aromatic region of the ^{1}H NMR spectrum of XAN in deuterated DMSO-d_6. The signal assignment is the following: H3, 6.889 ppm; H5, 7.542 ppm; H6, 7.303 ppm; H7, 7.133 ppm; $J_{5,6}$ = 8.4 Hz; $J_{5,7}$ = 1.1 Hz; $J_{6,7}$ = 7.8 Hz. No NMR signal has been detected in the aliphatic region of the spectrum, testifying that diketo structure XAN_{dk} (Scheme 1) is not present in the solution.

Commercially available deuterated DMSO contains traces of water, which can influence the tautomeric transformations of XAN. We also measured ^{1}H NMR spectra of XAN in DMSO-d_6 dried over molecular sieves (Fig. 3b). The shapes of NMR signals from H5 and H7 changed insignificantly, while the signals from H6 and especially from H3 underwent a strong line broadening. The width of the signals shows direct correlation with water content: in drier solvent the lines are broader. This result unambiguously testifies that in a polar aprotic solvent XAN exists in two tautomeric states, the transitions between states being mediated by the residual water (fast exchange). According to the results of DFT calculations (Table 1), these two forms are XAN_e and XAN_k (Scheme 1), which have the lowest and almost equal energies in DMSO.

NMR spectra were also recorded in aqueous neutral (pH 7.0) and basic (pH 11.0) solutions. The obtained spectra are similar to the spectrum shown in Fig. 3a, though the signal positions vary within 0.6 ppm depending on the pH of the solution. Again, the absence of signal in the aliphatic region testifies that the diketo structure XAN^-_{dk} is not present in noticeable amount in the XAN aqueous solution.

1.4 Tautomeric and acid–base equilibrium in XAN ground state. Our experimental data and theoretical calculations

Table 2 The fluorescence quantum yields (Φ_{fl}) of XAN at different excitation wavelengths. Standard error: 10%

Solvent	α^a	Φ_{fl}			
		λ_{exc} = 280 nm	λ_{exc} = 300 nm	λ_{exc} = 330 nm	λ_{exc} = 360 nm
H_2O, pH 1.0		<0.001	<0.001	<0.001	<0.001
H_2O, pH 6.0	1.17	0.001	0.001	0.001	0.001
H_2O, pH 12.0		0.003	0.003	0.006	0.006
MeOH	0.93	0.011	0.024	0.025	0.026
EtOH	0.83	0.053	0.064	0.061	0.051
DMF	0	—	0.021	0.013	0.10

[a] Solvatochromic parameter[49,50] characterizing the hydrogen-bonding ability of the solvent.

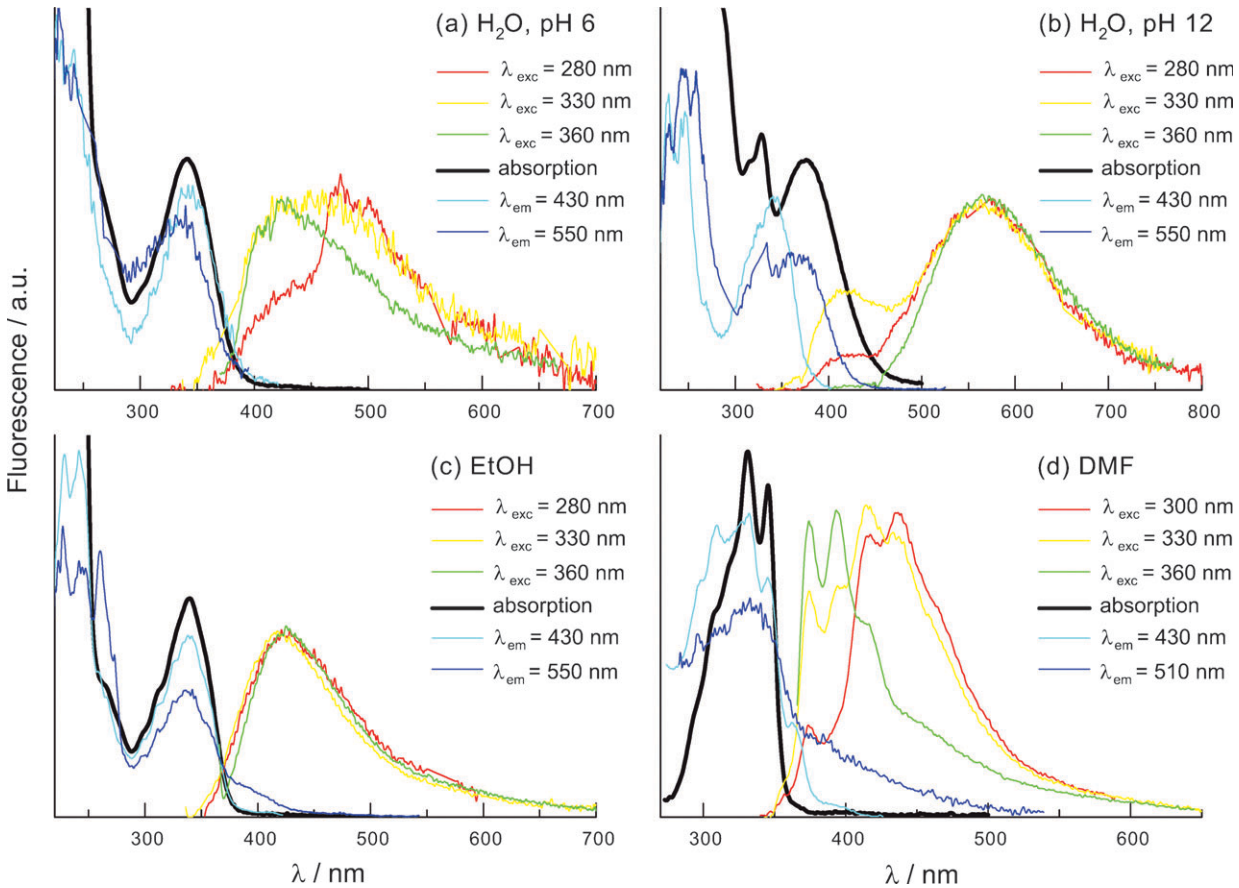

Fig. 2 Optical spectra of XAN aqueous solutions (a) pH 6 and (b) pH 12, (c) EtOH and (d) DMF at room temperature. Bold solid lines—absorption spectra; red, yellow and green lines—fluorescence emission spectra; cyan and blue lines—fluorescence excitation spectra. All spectra are normalized.

demonstrate that XAN in the ground state is rather sensitive to the environment. Under physiological conditions (*i.e.* in neutral aqueous solution) the major isomer is the keto form XAN^-_k, whose free energy is lower than the free energies of the other tautomeric forms (Table 1). However, in acidic and basic solutions, the free energy gap between the different tautomeric forms decreases down to 1–2 kcal mol^{-1}, and in aprotic polar solvents the enol and keto forms of XAN have almost equal energies. The combination of results obtained by fluorescence and NMR measurements as well as the quantum chemical calculations give strong evidence that in aprotic solvents XAN is present in two tautomeric forms, XAN_k and XAN_e. Fluorescence spectra also indicate that in basic solutions two forms of XAN, $XAN^{2-}{}_k$ and $XAN^{2-}{}_{e1}$, are probably present. It is important to note that the value of the second dissociation constant of XAN is 7.7, which means that at pH 7 about 20% of XAN is present in a dianionic state; thus, even in neutral aqueous solutions some minor admixture of the enol form is possible.

We have not found any evidence of the presence of the diketo form of XAN (XAN_{dk} or XAN^-_{dk}) in any of the solvents used. Theoretical calculations demonstrate that this form is the energetically least favorable one among the tautomeric structures of XAN. The lack of aliphatic signals in the NMR spectra of XAN confirms the absence of diketo form in aqueous and DMSO solutions. Thus, the previous assumption[25] about

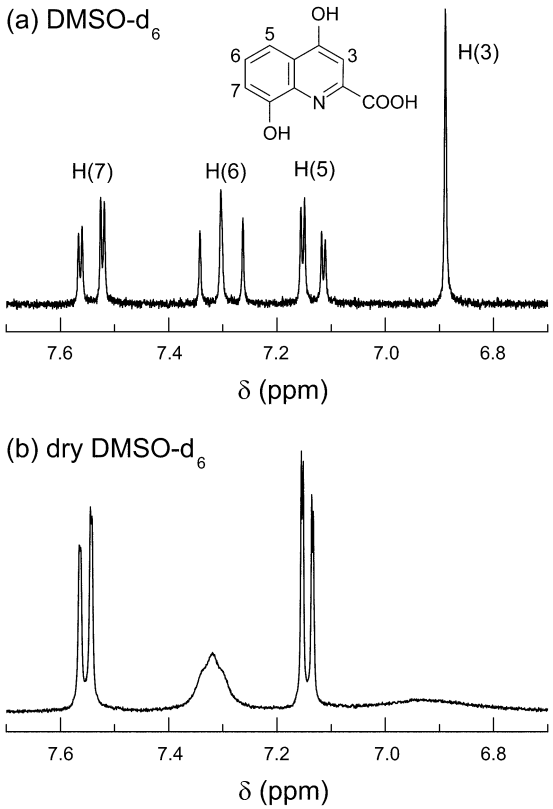

Fig. 3 Aromatic region of the ^{1}H NMR spectra of XAN in DMSO-d$_6$: (a) regular solvent, (b) the solvent dried over molecular sieves.

the presence of this form in alkaline solutions should be ruled out.

2 Early fluorescence and TA dynamics

2.1 Fluorescence up-conversion measurements. The temporal evolution of XAN fluorescence in H_2O (pH 5.3) has been measured at 8 wavelengths from 470 to 600 nm throughout the emission band over different time windows up to 100 ps (the excitation wavelength was 370 nm). Fig. 4 (upper picture) shows the first 40 ps of the fluorescence time profiles taken at 480, 540 and 600 nm; the same time profiles on a shorter time scale are presented in the bottom picture. At short wavelengths (near 480 nm), the fluorescence signal undergoes a fast decay. At longer wavelengths (around 540 nm), the decay becomes slower, and around 600 nm, one can see an initial signal growth followed by a relatively slower decay. The measured data were treated by global analysis using the sum of three exponential functions convolved with a Gaussian-like instrument response function as described in details in ref. 51,52. The best fit, shown by smooth lines in Fig. 4, was obtained with τ_1 = 0.6 ps, τ_2 = 1.5 ps, and τ_3 = 11 ps. The insert in Fig. 4 depicts the wavelength dependence of the amplitude factors associated with these time constants, $A_1(\lambda)$, $A_2(\lambda)$ and $A_3(\lambda)$. Positive values correspond to decays, and negative ones to the rises of the signal intensity.

These results can be interpreted as follows: at pH 5.3, XAN is present in the aqueous solution mostly in XAN^-_k (Scheme 1) form, and 370 nm excitation results in the population of the Franck–Condon first singlet excited state

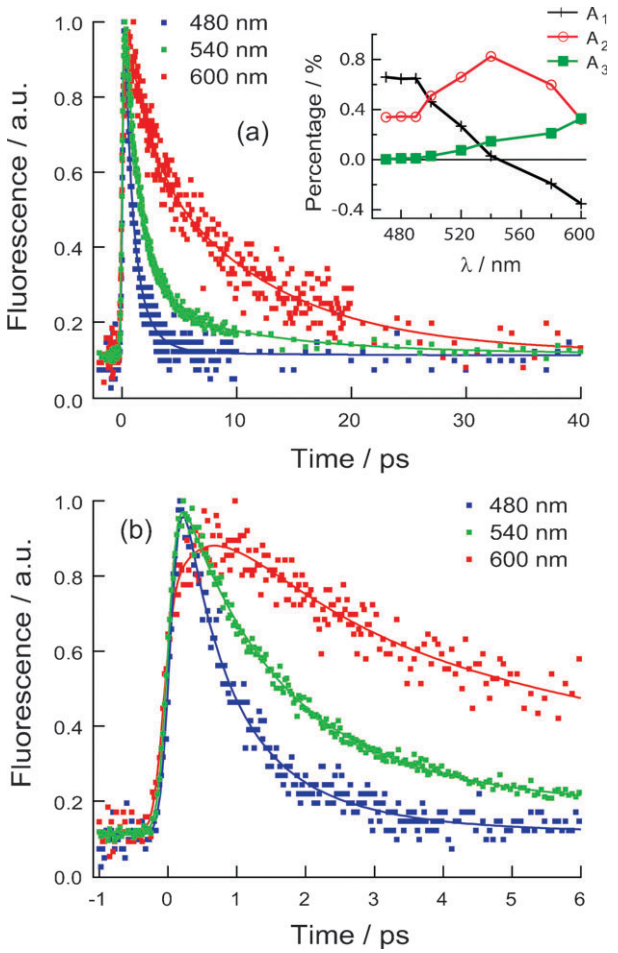

Fig. 4 Upper graph—fluorescence kinetics of XAN aqueous solution (pH 5.3) measured at 480, 540 and 600 nm, excitation at 370 nm; bottom graph—the same kinetics at a shorter time scale. Insert: amplitude spectra obtained from the global fit of the fluorescence time profiles.

^{S1}XAN^-_k*. The relaxation of ^{S1}XAN^-_k* to the thermal equilibrium involves mainly solvation that occurs in two steps: inertial motion of water molecules that occurs within 50–150 fs, and cannot be resolved with our setup, and diffusive motion of the solvent around the excited molecule that can be associated with the fastest component τ_1 of the fluorescence dynamics. Indeed, the spectrum of the amplitude factor $A_1(\lambda)$ exhibits a decay on the high-energy side and a rise on the low-energy side, which corresponds to a dynamic red shift. Furthermore, the obtained value of τ_1 is close to the values reported in literature[53,54] for reorientational motion of water.

The $A_2(\lambda)$ and $A_3(\lambda)$ components exhibit only positive values over the whole spectral region, and they are assigned to different emitting species. Excitation of XAN^-_k into S1 state leads to a redistribution of the electron density, which increases the acidity of the amino group and the basicity of the carbonyl group. Thus, the processes associated with the time constants τ_2 andτ_3 can be assigned to the two-step reaction of the keto-enol transformation—the protonation of the carbonyl oxygen and the deprotonation of the amino group. As a consequence, the second time constant τ_2 should be attributed to the decay of the singlet excited state ^{S1}XAN^-_k, and the

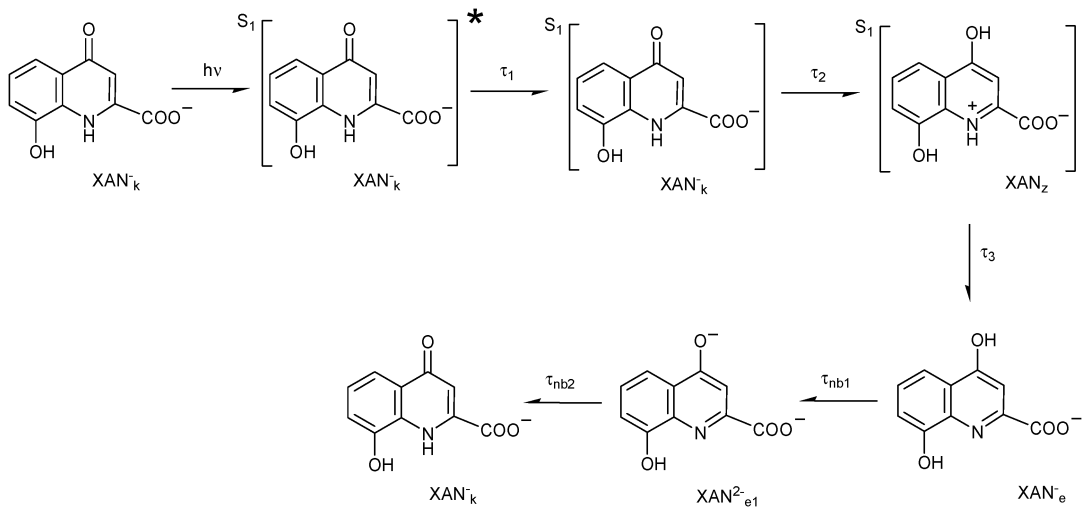

Scheme 2

third, τ_3, to the decay of the short-lived intermediate state formed after the first step of the reaction. From our data it is difficult to determine which reaction—proton attachment or proton loss—proceeds faster. However, since the intermediate state is fluorescent, one can conclude that after the first step of the reaction the molecule remains in the electronically excited singlet state, while the second step results in the formation of a non-fluorescent species (triplet or ground state). The possible mechanism of the S1 state deactivation is presented in Scheme 2. For simplicity, the proton attachment to the carbonyl group is depicted here as the first step.

We should note that the values of τ_1 and τ_2 are of the same order, and relatively good fit could be obtained when varying these parameters within 30–40%. Thus, the reported values of τ_1 and τ_2 should be considered as estimation.

XAN fluorescence dynamics was also measured in a water–MeOH mixture (1/1 by volume). The spectral evolution of the signal is similar to that in aqueous solution, but all time constants demonstrate a 2–3 fold increase, which indicates the crucial role of solvent in the S1 state deactivation process.

2.2 Femtosecond transient absorption measurements. Fig. 5a shows the transient absorption (TA) spectra recorded at different time delays after 400 nm excitation of XAN in aqueous solution. Similar results were obtained for buffered and non-buffered solutions, as well as for moderately acidic (pH 5.6) and basic (pH 11) conditions. Immediately after excitation, a TA band with a maximum at 510 nm is observed. The subsequent dynamics includes the formation of a shoulder in the 550–700 nm region during the first few picoseconds and a monotonic decay of the TA signal during the following 40 ps. The resulting signal—a broad band with an implicit maximum near 650 nm—remains unchanged up to 2 ns. The observed dynamics is additionally illustrated by time profiles of the TA signal at 510, 620 and 720 nm in Fig. 5b.

A global analysis of TA dynamics was performed using the following expression:

$$A(\lambda) = y_0(\lambda) + A_{1a}(\lambda) \times \exp(-t/\tau_{1a}) + A_{2a}(\lambda) \times \exp(-t/\tau_{2a}) \quad (1)$$

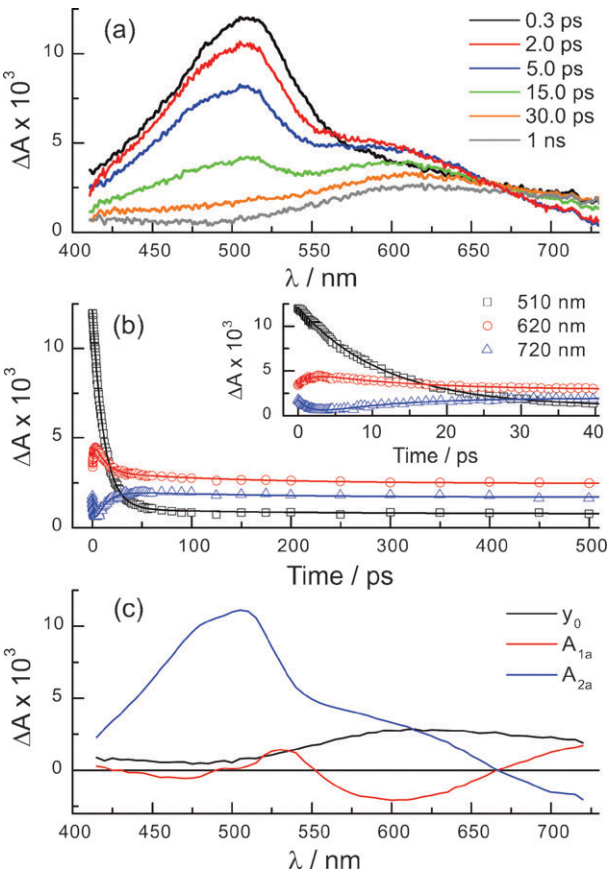

Fig. 5 TA dynamics of XAN aqueous solution (pH 5.6) observed after laser pulse excitation (400 nm, 150 fs, 3 μJ). (a) TA spectra recorded at different time delays after excitation. (b) TA time profiles measured at 510, 620 and 720 nm; solid lines show best fit; insert shows early dynamics at the same wavelengths. (c) decay-associated amplitude spectra obtained from the global analysis of the TA time profiles.

The best fit (smooth lines in Fig. 5b) gives time constants τ_{1a} and τ_{2a}; the obtained values for buffered and non-buffered solutions and for acidic and basic conditions are similar, the averaged values being $\tau_{1a} = 1.4 \pm 0.5$ ps and $\tau_{2a} = 12.9 \pm 1.5$ ps.

The associated amplitude spectra, $y_0(\lambda)$, $A_{1a}(\lambda)$ and $A_{2a}(\lambda)$, are presented in Fig. 5c; positive values correspond to a decay, and negative ones to a rise of the intensity. The spectrum associated with the fastest component, $A_{1a}(\lambda)$, exhibit two alternating positive-negative bands. Taking into account the results of the fluorescence up-conversion measurements (see above), this component should be attributed to the superposition of the solvent-induced dynamics Stokes shift of the absorption bands of the species formed after UV excitation, and to the decay of the photoexcited $^{S1}XAN^{-}{}_{k}$ with the formation of a short-lived fluorescent intermediate (the first step of the solvent-assisted tautomeric transformation of $^{S1}XAN^{-}{}_{k}$, Scheme 2). The spectrum of the second component, $A_{2a}(\lambda)$, is similar to the TA spectrum observed after completion of the initial spectral dynamics, and the associated time constant τ_{2a} can be interpreted as the decay time of the fluorescent intermediate formed after the first step of the reaction. The negative signal at $\lambda > 650$ nm should be attributed to the $S_1 \rightarrow S_0$ stimulated emission because $XAN^{-}{}_{k}$ exhibits a broad fluorescence band (Fig. 2b). The residual spectrum, $y_0(\lambda)$, corresponds to a superposition of spectra of the relatively long-lived intermediates. In particular, the signal in 500–730 nm region may be attributed to the absorption of the solvated electron $e_{aq}{}^{-}$, which has been reported to have a maximum at 720 nm.[55]

In order to clarify the nature of the long-lived signal on the red side of the $y_0(\lambda)$ spectrum, additional experiments were performed in basic media (non-buffered solution, pH 11), where the yield of the solvated electron is higher. First, the laser energy dependence of the TA intensity was measured at 620 nm, 1.5 ns after excitation. A quadratic dependence can clearly be seen (see ESI†), indicating that the formation of this species is a biphotonic process. Second, the photolysis of XAN was performed in the presence of 1.1 M acetone (electron scavenger). Under these conditions, the decay of the solvated electron should occur with a characteristic time of about 150 ps ($k_{SC} = 6.5 \times 10^9$ M^{-1} s^{-1}).[56] Indeed, the global analysis of TA spectra obtained in the presence of acetone with the sum of three exponents (one additional exponent in expression (1)) gives time constants $\tau_{1a} = 1.4$ ps, $\tau_{2a} = 17.3$ ps and $\tau_{3a} = 149$ ps; the $y_0(\lambda)$ spectrum exhibits zero values over the whole wavelength region. The first two time constants are similar to those obtained in the absence of acetone; the latter agrees perfectly with the estimated value of 150 ps. Finally, the TA spectrum of the solvated electron was measured in a separate experiment, namely upon excitation at 266 nm of a solution of triethylamine in water. The obtained spectrum coincides very well with that obtained 1 ns after the excitation of XAN aqueous solution (Fig. 5a). Thus, the observed long-lived signal can be assigned to the solvated electron. The discrepancy between previously reported value of the solvated electron absorption maximum (720 nm) and that observed in our measurements (620–650 nm) can most probably be ascribed to the chromatic aberration of the set-up, that could lead to spectral distortion. The laser pulse energy dependence of the TA absorption and the TA profiles obtained in the presence of acetone are presented in the ESI.†

Summarizing the results obtained with the use of fluorescence up-conversion and femtosecond TA methods, the following processes contribute in the early dynamics of photoexcited XAN molecule: (a) solvent relaxation occurs within 1 ps (τ_1) and causes the red shift of both fluorescence emission band and TA band; (b) the deactivation of S1 state in aqueous solutions proceeds in two steps with the characteristic time constants of about 1.5 ps (τ_2 in fluorescence measurements and τ_{1a} in TA measurements) and about 12 ps (τ_3 in fluorescence measurements and τ_{2a} in TA measurements). These two steps are the protonation of the carbonyl group and the deprotonation of the amino group; from our results, it is difficult to determine which one of these reactions occurs earlier.

3 Nanosecond laser flash photolysis (LFP)

3.1 266 nm photolysis of XAN aqueous solutions. Fig. 6 shows transient absorption spectra obtained under 266 nm photolysis of an aqueous XAN solution (1.26×10^{-4} M, pH 7.0) 40 ns and 1 μs after the laser flash. The analysis of the time evolution of the transient absorption (inserts in Fig. 6) indicates that at least three intermediates are observed. The signal observed at the low-energy side of the spectra decays exponentially with an observed rate constant proportional to the XAN concentration, $k_{obs} = k_0 + k_e \times [XAN]$. The calculated second-order rate constant $k_e = (2.1 \pm 0.5) \times 10^{10}$ M^{-1} s^{-1} is in a good agreement with the rate constant of the capture of the solvated electron by xanthurenic acid.[34] The signal disappears in the presence of the electron scavenger acetone. Therefore, this signal was attributed to the solvated electron formed upon photoionization of $XAN^{-}{}_{k}$. The photoionization quantum yield was calculated using the absorption coefficient of the solvated electron at 600 nm $\varepsilon_{600} = 1.4 \times 10^4$ M^{-1} cm^{-1}.[55] The initial optical density of the solvated electron absorption shows a quadratic dependence on the laser power, which corresponds to a linear dependence of the photoionization quantum yield (Fig. 7), and testifies that the ionization proceeds *via* a biphotonic mechanism.

The absorption around 450 nm and below 320 nm (Fig. 6) decays much more slowly by second-order kinetics. The initial intensities of these signals also exhibit a quadratic dependence on the laser intensity. These signals were attributed to the superposition of $XAN^{\bullet}$ radical and electron adduct, formed upon ionization of the starting compound followed by the capture of the electron by $XAN^{-}{}_{k}$ in the ground state.

An intermediate X with absorption bands in the 370–430 nm region (maximum at 400 nm) and below 300 nm undergoes a exponential decay with a time constant of 29 ± 5 ns. This time constant does not depend on the initial XAN concentration. The intensity of the signal due to X is proportional to the laser pulse energy, *i.e.* this intermediate is formed in a monophotonic process. The assignment of this signal will be discussed below.

The negative absorption with a maximum at about 340 nm corresponds to the depletion of the starting material. The evolution of this signal occurs on different time domains. The very fast initial decay of the negative absorption proceeds with the same rate as the decay of the intermediate X monitored at 400 nm (see inserts in Fig. 6), indicating that the decay of the intermediate X results in the recovery of the starting material. The following increase of the negative

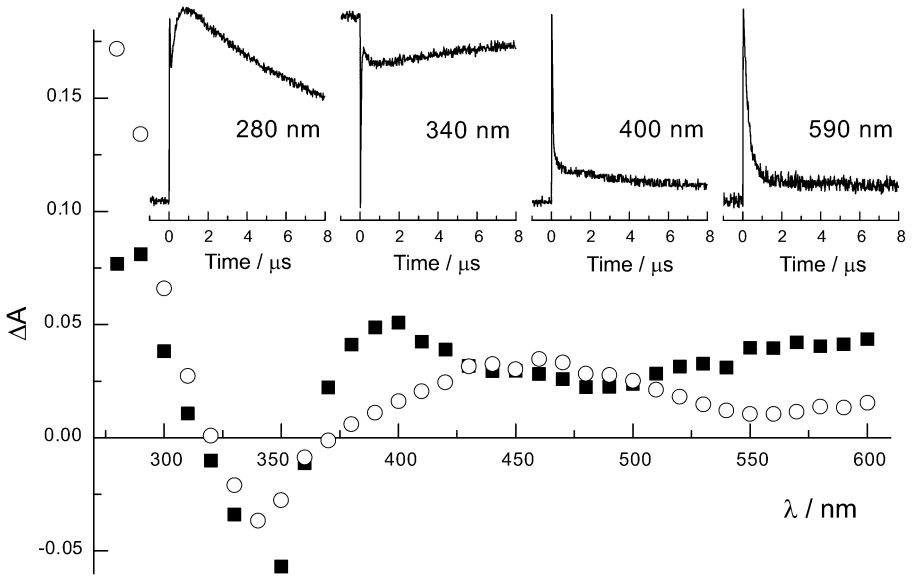

Fig. 6 Transient absorption spectra detected 40 ns (squares) and 1 μs (circles) after the laser pulse irradiation (266 nm, 40 mJ) of XAN neutral aqueous solution. Inserts show the time profiles at selected wavelengths.

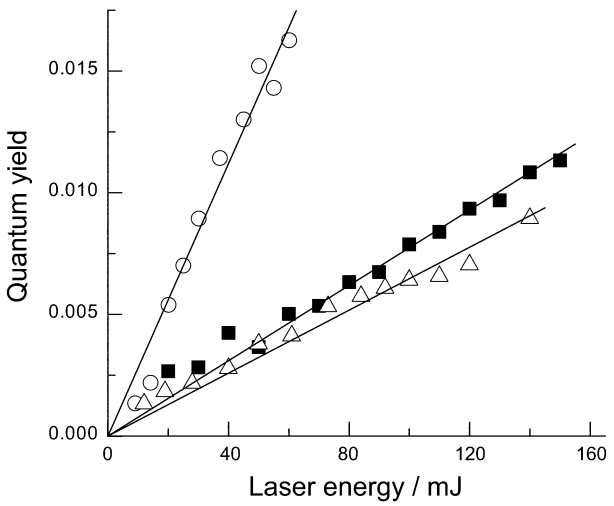

Fig. 7 Dependence of the quantum yield of XAN photoionization on laser energy. Circles—aqueous neutral solution, excitation at 266 nm; squares—aqueous neutral solution, excitation at 355 nm; triangles—methanol, excitation at 355 nm.

absorption at 340 nm within approximately 0.5 μs corresponds to the consumption of XAN^-_k due to the formation of the electron capture adduct. Finally, the slow decay of the negative absorption corresponds to the restoration of the initial compound in the radical recombination reactions.

In the presence of oxygen, no substantial changes in the transient absorption spectra or kinetics have been observed, indicating that XAN^-_k excitation in aqueous solution does not result in triplet state population.

3.2 355 nm photolysis of XAN aqueous solutions. The transient absorption spectra obtained under 355 nm flash photolysis of 1.8×10^{-4} M XAN aqueous neutral solutions are similar to those observed under 266 nm photolysis, and point to the formation of the same short-lived intermediates: solvated electron, $XAN^{\bullet}$ radical and electron adduct formed upon biphotonic ionization of XAN^-_k, and the intermediate X, formed in a monophotonic process. The most significant difference between the results obtained upon 266 nm and 355 nm excitations is the relative contribution of the biphotonic ionization: with the same laser intensity, the solvated electron yield is much higher upon 266 nm photolysis (Fig. 7). To avoid complications in data interpretation caused by biphotonic processes, all further experiments were performed at low laser energies and in the presence of 10^{-2} M acetone (electron scavenger, the rate constant of the electron addition to acetone[56] is 6.5×10^9 M^{-1} s^{-1}). Under such conditions, the intermediate X with the absorption maximum at 400 nm was the only species observed in the photolysis (Fig. 8).

The kinetics and the initial intensity of the transient absorption monitored at 400 nm does not change in the presence of acetone or oxygen, indicating that the intermediate X is neither a triplet state nor a product of solvated electron reactions. However, the signal decay rate strongly depends on the solution acidity, the decay accelerating at low pH. It has also been noticed that even at the same pH, the signal decay in buffered solutions is significantly faster than in non-buffered aqueous solutions. Moreover, in all buffered solutions, the kinetic traces were well reproduced by an exponential function, while in non-buffered solutions the decay of the signal can be considered as monoexponential only at low pH values. Above pH 4, a satisfactory agreement between experimental and calculated kinetics was achieved only with the use of a biexponential function with time constants τ_{nb1} and τ_{nb2}. The obtained pH dependences of the time constants of the intermediate X decay in buffered (τ_b) and non-buffered (τ_{nb1} and τ_{nb2}) solutions are presented in Fig. 9. All presented values of τ_b and the values of τ_{nb1} below pH 3.9 are the results of a monoexponential fit, while the values of τ_{nb1} above pH 3.9 and the values of τ_{nb2} were obtained by biexponential fitting.

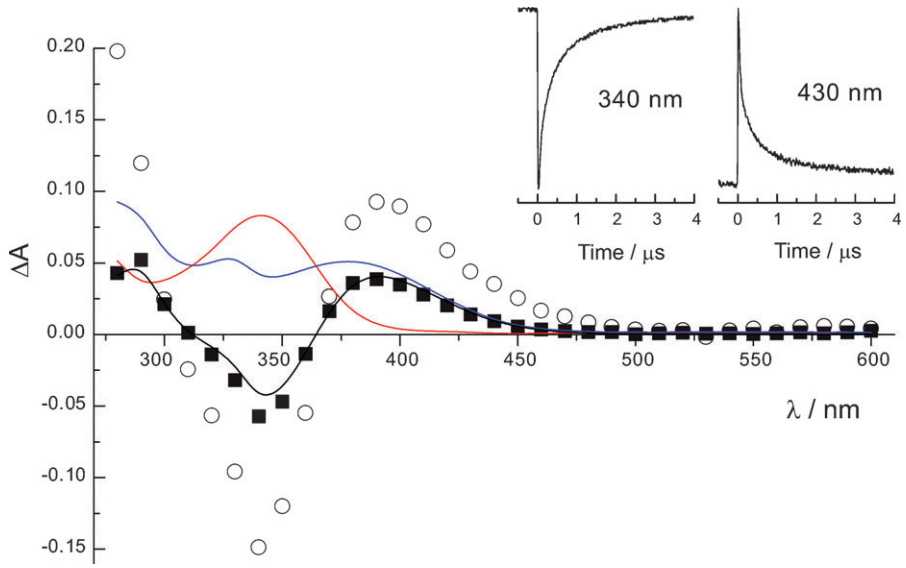

Fig. 8 Transient absorption spectra obtained 50 ns (circles) and 200 ns (squares) after the laser pulse irradiation (355 nm, 30 mJ) of XAN neutral non-buffered aqueous solution. Inserts show the time profiles at selected wavelengths. Red line—electronic spectrum of 1.2×10^{-5} M XAN neutral solution, blue line—electronic spectrum of 1.2×10^{-5} M XAN basic solution, black line—the difference spectrum.

The obtained values confirm that the signal decay in buffered solution is much faster: for example, at pH 6.7 the obtained values are $\tau_b = 35$ ns (for buffered solution), and $\tau_{nb1} = 120$ ns, $\tau_{nb2} = 714$ ns (for non-buffered solution).

The biexponential decay of the transient absorption at 400 nm and the corresponding biexponential recovery of the starting material in non-buffered solutions (see inserts in Fig. 8) show that the transformation of the intermediate X into the starting XAN^-_k proceeds in two stages. Thus, the intermediate X is assigned to the tautomeric form of xanthurenic acid, XAN^-_e, formed within the duration of the laser pulse due to isomerisation of the photoexcited $^{S1}XAN^-_k$. Correspondingly, the two observed stages of the starting compound recovery (Scheme 2) include the deprotonation of the hydroxyl group of XAN^-_e (faster and almost pH independent process, τ_{nb1}) and the protonation of the nitrogen atom (τ_{nb2}). The simplest reaction chain leading to the restoration of the starting $^{S0}XAN^-_k$ form is presented in Scheme 2, although other pathways cannot be excluded.

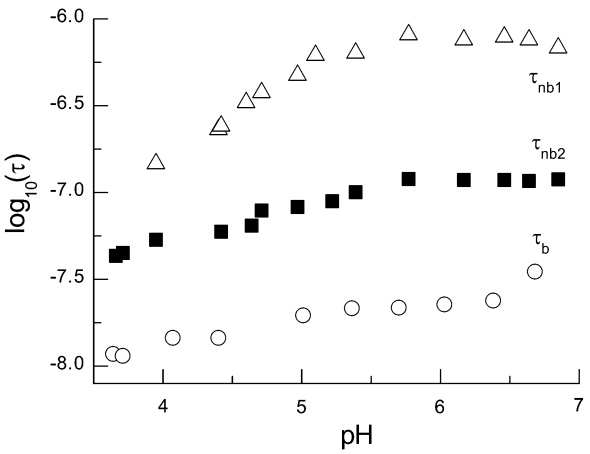

Fig. 9 pH dependences of the time constants of TA decay, monitored at 400 nm after 355 nm laser pulse irradiation of XAN aqueous solutions. Circles—buffered solution, monexponential fit (τ_b); squares and triangles—non-buffered solution, biexponential fit (τ_{nb1} and τ_{nb2}).

The comparison of the LFP data and the steady-state optical absorption spectra supports the proposed kinetic scheme (Scheme 2). The smooth lines in Fig. 8 show the absorption spectra of XAN in basic (pH 9.5, blue line) and neutral (pH 6.5, red line) solutions, as well as the difference between these two spectra. The latter almost perfectly coincides with the transient absorption spectrum (squares) obtained 200 ns after the laser irradiation of non-buffered XAN solution, testifying that indeed deprotonated xanthurenic acid XAN^{2-} is a short-lived intermediate of XAN photolysis in aqueous solutions.

3.3 355 nm photolysis of XAN solutions in alcohols. The spectra obtained upon XAN photolysis in MeOH and EtOH are very similar to those observed in aqueous solutions. The photoionization yield is also very similar to that in aqueous solution (Fig. 7). At low laser energies, the only product observed is XAN^-_e, its absorption maximum is red-shifted to 420 nm in MeOH and to 410 nm in EtOH. As in aqueous solutions, the rate of the XAN^-_e decay (monitored at 410 nm) was equal to the rate of the starting compound restoration (monitored at 345 nm) and did not depend on the presence of acetone or oxygen in the solution. However, the time constants of the signal decay in alcohols are significantly higher than in aqueous solution: 480 ± 50 ns in MeOH and 141 ± 12 ns in EtOH (monoexponential fit).

We also performed the measurements of XAN^-_e decay in mixtures of MeOH and aqueous neutral (pH 7.0) buffer. The time constant of the signal decay was 77 ns in 20% MeOH mixture and 172 ns in 50% MeOH mixture. As expected, the observed time constant increases as the MeOH content in the mixture is increased.

3.4 355 nm photolysis of XAN solutions in DMF and DMSO. LFP of XAN in the aprotic solvents DMF and

DMSO, as well as in aqueous and alcoholic solutions, results in biphotonic ionization; thus, the experiments were performed at low laser energies and in the presence of 10^{-2} M of the electron scavenger acetone.

Fig. 10 and 11 show transient absorption spectra obtained 200 ns after the laser excitation of 1.7×10^{-4} M XAN solution in DMF photolysis saturated with argon and with oxygen, respectively. Since the broad intense band with a maximum at 560 nm and the strong transient absorption ranging from 280 to 320 nm are readily quenched by oxygen, these signals were attributed to XAN triplet state (^{T}XAN). Inspection of the kinetic curves of ^{T}XAN decay under anaerobic conditions (inserts in Fig. 10, traces at 560 nm and 580 nm) demonstrates that the rate of the triplet decay depends on the observation wavelength. This testifies that the triplet state is present in solution in more than one tautomeric form. Since our steady-state spectroscopic experiments (see above) demonstrated that in polar aprotic solvents XAN is present in both enol XAN_e and keto XAN_k forms, one can assume that the two forms of the triplet state also correspond to enol and keto forms. The decay of triplet states is not accompanied by the signal growth at any wavelength (except near 350 nm, the absorption maximum of the starting compound), which likely means that the main channels of the triplet states decay are triplet annihilation (at high triplet concentrations) or quenching by traces of oxygen or other impurities (at low triplet concentrations).

The transient absorption spectrum recorded upon LFP of oxygen-saturated solutions (Fig. 11) corresponds to the short-lived intermediates formed simultaneously with the triplet states, *i.e.* their precursors are singlet excited states of XAN in both enol and keto forms. The kinetics observed at different wavelengths (inserts in Fig. 11) shows that several species contribute to the spectrum. The shapes of the kinetic curves do not change with the variation of the concentration of the starting compound or laser intensity. Most likely, these spectral changes are due to the tautomeric transformations of different forms of XAN in the ground state. The analysis of the kinetic curves shows that at least three intermediates participate in the reaction; however, due to the strong spectral overlap, it is difficult to separate the contributions of individual species to the total transient absorption spectrum (Fig. 11) and to suggest an unambiguous reaction scheme.

Similar spectra and kinetics have been observed upon LFP of DMSO solutions of XAN, which testifies that the reactions in both aprotic solvents proceed in a similar way.

3.5 Photoionization of XAN. Under intense laser irradiation, XAN undergoes biphotonic ionization. During the photolysis of XAN in aqueous and alcohol solutions, the population of the triplet state does not occur, so the possible precursors for photoionization are the first singlet excited state and the short-lived photochemically produced tautomeric form of XAN (XAN^-_e) in the ground state. The probability of absorption by photochemically produced species during the laser pulse, and, correspondingly, the photoionization quantum yield depends on the lifetime of these species. The intensity of the solvated electron signal is the same in aqueous buffered, aqueous non-buffered, and methanol solutions (Fig. 7), although the lifetimes of the unstable tautomeric structures in these solvents differ significantly. Thus, one can conclude that the precursor for XAN photoionization is the singlet excited state. This conclusion is supported by femtosecond TA measurements: the absorption of the solvated electron appears in the spectrum immediately after the laser pulse, indicating that the precursor for ionization is formed within the duration of the laser pulse (approximately 150 fs).

3.6 Photochemically induced transformations of XAN. The present results demonstrate that the major decay channel of photoexcited $^{S1}XAN^-_k$ in aqueous and alcohol solutions is the conversion into its ground state tautomeric form, XAN^-_e.

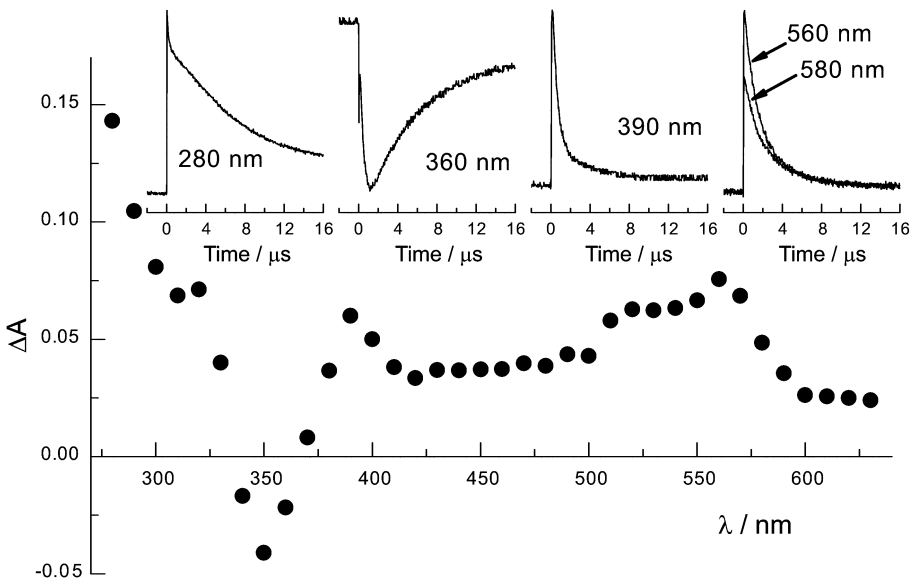

Fig. 10 Transient absorption spectrum obtained 200 ns after the laser pulse irradiation (355 nm) of XAN solution in DMF under argon. Inserts show the time profiles at selected wavelengths.

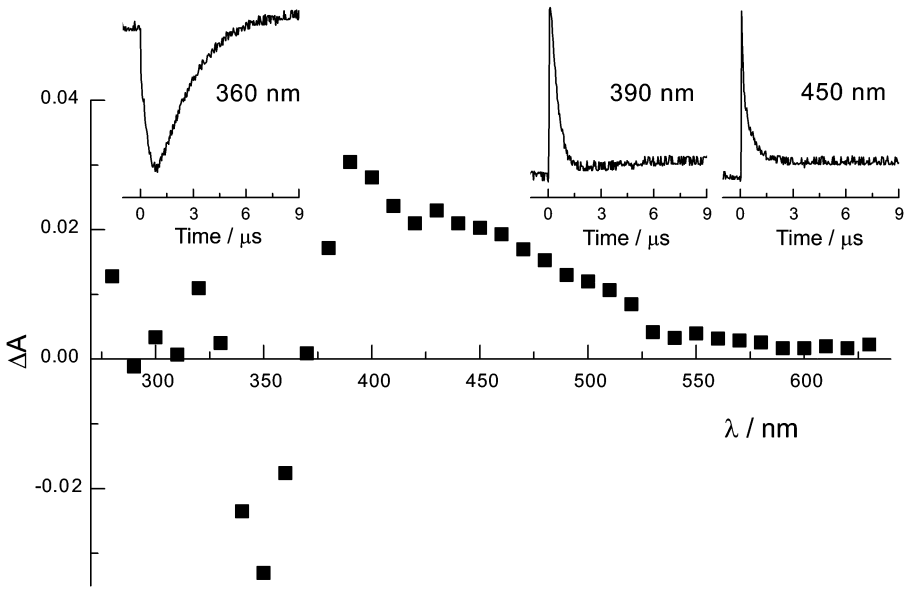

Fig. 11 Transient absorption spectrum obtained 200 ns after the laser pulse irradiation (355 nm) of XAN solution in DMF under oxygen. Inserts show the time profiles at selected wavelengths.

Apparently, the driving force for this transformation is an increase of the electron density on the carbonyl group upon excitation, which increases the acidity of the amino group and the basicity of the carbonyl group. Fluorescence up-conversion and femtosecond TA measurements demonstrate that the deactivation of the fluorescent S1 state proceeds in two steps-the protonation of the carbonyl oxygen and the deprotonation of the amino group. Taking into account that both protonation and deprotonation reactions occur on the picosecond time scale, one can conclude that the solvent molecules are directly involved in the proton transfer reactions—in other words, in the excited molecule $^{S1}XAN^{-}_{k}$, the carbonyl group is more basic and the amino group more acidic than the solvent. A similar mechanism of S_1 state deactivation has been recently reported[57] for the metabolic precursor of XAN, kynurenine (KN), which plays the role of UV filter in mammalian eye lenses. The major difference in the photochemical behaviors of KN and XAN is that the deactivation of ^{S1}KN yields the starting molecule in the ground state, whereas the decay of $^{S1}XAN^{-}_{k}$ results in the formation of its enol form in the ground state. The suggested mechanism explains the low fluorescence quantum yield of XAN (this work and ref. 25 and 28), as well as the very low quantum yield (below 10^{-5}) of the anaerobic decomposition of XAN.[6]

The decay of $^{S1}XAN^{-}_{k}$ and, correspondingly, the formation of XAN^{-}_{e} in aqueous solutions proceed on the picosecond time scale. The spectrum of XAN^{-}_{e} was recorded with the use of nanosecond LFP; however, we were only able to observe the tail of XAN^{-}_{e} absorption (420–470 nm, Fig. 5a, gray line) in the pump–probe transient absorption measurements. The TA dynamics in the 350–390 nm range is hidden by the strong absorption of the initial compound, and in the 390–410 nm range—by the strong signal from the 400 nm pump pulse. Thus, only the most absorbing species—the excited singlet state $^{S1}XAN^{-}_{k}$ and the solvated electron—are reliably detected in these measurements.

In DMF and DMSO, the photochemical properties of XAN change dramatically. In these aprotic solvents, deprotonation does not take place, so XAN is present not in an anionic but in a neutral form. Due to the absence of hydrogen bonding with the solvent molecules, the energy levels of the keto and enol states become approximately equal, so both forms are present in solutions. Most importantly, the photoexcited XAN cannot undergo proton transfer reactions in aprotic solvents. Thus, the major decay channel of the S_1 state in water and alcohols—the solvent-assisted conversion into ground enol form—does not operate in DMF and DMSO, which leads instead to the formation of short-lived intermediate forms of XAN both in the triplet and ground states. The mechanism of tautomeric transformations of XAN in aprotic solvents remains uncertain. One possible explanation is the participation of residual water molecules in the reaction. However, the test measurements revealed that the addition of water (up to 1%) into DMF solutions of XAN does not influence the signal intensities or kinetics observed by transient absorption. Thus, the most plausible mechanism is the intramolecular proton transfer between protropic groups of XAN in excited and ground states. This reaction is much slower than the intermolecular proton transfer in protic solvents, and therefore the lifetime of the S_1 state and the fluorescence intensity in aprotic solvents increase significantly. From a biological viewpoint, if XAN is indeed produced inside the lens, one can expect that in the protein-rich and highly ordered environment of the lens, the conditions are less protic than in an aqueous solution, especially if XAN is attached to the lens proteins. This may result in an increase of the yield of reactive intermediates upon XAN photoexcitation and protein photo-oxidation.

Conclusions

Proton transfer between XAN and solvent molecules is the key reaction determining the photostability of XAN: the major

channel of photoexcited XAN decay in neutral aqueous and alcohol solutions is the solvent-assisted tautomerization into the enol form, followed by the solvent-assisted return into the initial keto form. The first reaction is pH independent and very fast, indicating that the solvent molecules are the direct proton donors. The back ground state enol → keto tautomerization proceeds in two steps (deprotonation of the hydroxyl group and protonation of the nitrogen atom), and the rate of these processes strongly depends on the acidity of the solution. In the absence of proton donors (aprotic solvents) the lifetime of the photoexcited S_1 state increases dramatically, and other decay channels—fluorescence, intersystem crossing and intramolecular proton transfer—become dominant.

Acknowledgements

This work was supported by the following agencies: FASI state contracts 02.512.11.2278, 02.740.11.0262 and P708, Russian Foundation for Basic Research (projects 08-03-00539 and 09-04-12135), President of the Russian Federation (grant NSh-7643.2010.3) the Division of Chemistry and Material Science, Russian Academy of Sciences, and SNF (Project Nr. 200020-115942). PSS thanks the European Scientific Foundation (DYNA Exchange Grant #1929). Support of this work by the Siberian Supercomputer Center is gratefully acknowledged.

References

1 R. van Heyningen, *Ciba Found. Symp.*, 1973, **19**, 151–171.
2 A. M. Wood and R. J. W. Truscott, *Exp. Eye Res.*, 1993, **56**, 317–325.
3 D. Balasubramanian, *Photochem. Photobiol.*, 2005, **81**, 498–501.
4 L. M. Taylor, J. A. Aquilina, J. F. Jamie and R. J. W. Truscott, *Exp. Eye Res.*, 2002, **75**, 165–175.
5 Yu. P. Tsentalovich, O. A. Snytnikova, M. D. E. Forbes, E. I. Chernyak and S. V. Morozov, *Exp. Eye Res.*, 2006, **83**, 1439–1445.
6 P. S. Sherin, Y. P. Tsentalovich, O. A. Snytnikova and R. Z. Sagdeev, *J. Photochem. Photobiol., B*, 2008, **93**, 127–132.
7 J. Dillon, R. H. Wang and S. J. Atherton, *Photochem. Photobiol.*, 1990, **52**, 849–854.
8 B. D. Hood, B. Garner and R. J. W. Truscott, *J. Biol. Chem.*, 1999, **274**, 32547–32550.
9 S. Vazquez, J. A. Aquilina, J. F. Jamie, M. M. Sheil and R. J. W. Truscott, *J. Biol. Chem.*, 2002, **277**, 4867–4873.
10 R. J. W. Truscott, *Int. J. Biochem. Cell Biol.*, 2003, **35**, 1500–1504.
11 R. J. W. Truscott, *Exp. Eye Res.*, 2005, **80**, 709–725.
12 N. R. Parker, J. F. Jamie, M. J. Davies and R. J. W. Truscott, *Free Radical Biol. Med.*, 2004, **37**, 1479–1489.
13 Yu. P. Tsentalovich, O. A. Snytnikova and R. Z. Sagdeev, *Russ. Chem. Rev.*, 2008, **77**, 789–797.
14 Yu. P. Tsentalovich, O. A. Snytnikova, P. S. Sherin and M. D. E. Forbes, *J. Phys. Chem. A*, 2005, **109**, 3565–3568.
15 O. A. Snytnikova, P. S. Sherin, L. V. Kopylova and Yu. P. Tsentalovich, *Russ. Chem. Bull.*, 2007, **56**, 732–738.
16 L. M. Taylor, J. A. Aquilina, J. F. Jamie and R. J. W. Truscott, *Exp. Eye Res.*, 2002, **74**, 503–511.
17 J. A. Aquilina, J. A. Carver and R. J. W. Truscott, *Exp. Eye Res.*, 1997, **64**, 727–735.
18 J. A. Aquilina, J. A. Carver and R. J. W. Truscott, *Biochemistry*, 2000, **39**, 16176–16184.
19 J. A. Aquilina and R. J. W. Truscott, *Biochem. Biophys. Res. Commun.*, 2000, **276**, 216–223.
20 J. A. Aquilina and R. J. W. Truscott, *Biochim. Biophys. Acta, Protein Struct. Mol. Enzymol.*, 2002, **1596**, 6–15.
21 B. Garner, D. C. Shaw, R. A. Lindner, J. A. Carver and R. J. W. Truscott, *Biochim. Biophys. Acta, Protein Struct. Mol. Enzymol.*, 2000, **1476**, 265–278.
22 L. V. Kopylova, O. A. Snytnikova, E. I. Chernyak, S. V. Morozov and Yu. P. Tsentalovich, *Exp. Eye Res.*, 2007, **85**, 242–249.
23 J. Mizdrak, P. G. Hains, R. J. W. Truscott, J. F. Jamie and M. D. Davies, *Free Radical Biol. Med.*, 2008, **44**, 1108–1119.
24 H. Z. Malina and X. D. Martin, *Graefe's Arch. Clin. Exp. Ophthalmol.*, 1995, **233**, 38–44.
25 H. Z. Malina and X. D. Martin, *Graefe's Arch. Clin. Exp. Ophthalmol.*, 1996, **234**, 723–730.
26 H. Z. Malina, *Biochem. Biophys. Res. Commun.*, 1999, **265**, 600–605.
27 E. Shirao, K. Ando, A. Inoue, Y. Shirao and D. Balasubramanian, *Exp. Eye Res.*, 2001, **73**, 421–431.
28 G. Thiagarajan, E. Shirao, K. Ando, A. Inoue and D. Balasubramanian, *Photochem. Photobiol.*, 2002, **76**, 368–372.
29 P. G. Hains, L. Gao and R. J. W. Truscott, *Exp. Eye Res.*, 2003, **77**, 547–553.
30 E. Bardez, A. Chatelain, B. Larrey and B. Valeur, *J. Phys. Chem.*, 1994, **98**, 2357–2366.
31 H. Yu, H.-L. Kwon and D.-L. Jang, *Bull. Korean Chem. Phys.*, 1997, **18**, 156–161.
32 T. G. Kim, T. J. Yoon and D. J. Jang, *Bull. Korean Chem. Phys.*, 1997, **18**, 467–469.
33 O. Poizat, E. Bardez, G. Buntinx and V. Alain, *J. Phys. Chem. A*, 2004, **108**, 1873–1880.
34 J. E. Roberts, J. F. Wishart, L. Martinez and C. F. Chignell, *Photochem. Photobiol.*, 2000, **72**, 467–471.
35 C. M. Krishna, S. Uppuluri, P. Riesz, J. S. Zigler and D. Balasubramanian, *Photochem. Photobiol.*, 1991, **54**, 51–58.
36 L. Shen and H.-F. Ji, *Dyes Pigm.*, 2008, **76**, 646–649.
37 J. E. Roberts, E. L. Finley, S. A. Patat and K. L. Schey, *Photochem. Photobiol.*, 2001, **74**, 740–744.
38 J. W. Eastman, *Photochem. Photobiol.*, 1967, **6**, 55–72.
39 I. F. Molokov, Yu. P. Tsentalovich, A. V. Yurkovskaya and R. Z. Sagdeev, *J. Photochem. Photobiol., A*, 1997, **110**, 159–165.
40 Yu. P. Tsentalovich, L. V. Kulik, N. P. Gritsan and A. V. Yurkovskaya, *J. Phys. Chem. A*, 1998, **102**, 7975–7980.
41 G. Duvanel, N. Banerji and E. Vauthey, *J. Phys. Chem. A*, 2007, **111**, 5361–5369.
42 A. Morandeira, L. Engeli and E. Vauthey, *J. Phys. Chem. A*, 2002, **106**, 4833–4837.
43 A. D. Becke, *J. Chem. Phys.*, 1993, **98**, 5648–5652.
44 C. Lee, W. Yang and R. G. Parr, *Phys. Rev. B: Condens. Matter*, 1988, **37**, 785–789.
45 P. S. Sherin, N. P. Gritsan and Yu. P. Tsentalovich, *Photochem. Photobiol. Sci.*, 2009, **8**, 1550–1557.
46 M. J. Frisch, G. W. Trucks, H. B. Schlegel, G. E. Scuseria, M. A. Robb, J. R. Cheeseman, J. A. Montgomery, Jr., T. Vreven, K. N. Kudin, J. C. Burant, J. M. Millam, S. S. Iyengar, J. Tomasi, V. Barone, B. Mennucci, M. Cossi, G. Scalmani, N. Rega, G. A. Petersson, H. Nakatsuji, M. Hada, M. Ehara, K. Toyota, R. Fukuda, J. Hasegawa, M. Ishida, T. Nakajima, Y. Honda, O. Kitao, H. Nakai, M. Klene, X. Li, J. E. Knox, H. P. Hratchian, J. B. Cross, V. Bakken, C. Adamo, J. Jaramillo, R. Gomperts, R. E. Stratmann, O. Yazyev, A. J. Austin, R. Cammi, C. Pomelli, J. Ochterski, P. Y. Ayala, K. Morokuma, G. A. Voth, P. Salvador, J. J. Dannenberg, V. G. Zakrzewski, S. Dapprich, A. D. Daniels, M. C. Strain, O. Farkas, D. K. Malick, A. D. Rabuck, K. Raghavachari, J. B. Foresman, J. V. Ortiz, Q. Cui, A. G. Baboul, S. Clifford, J. Cioslowski, B. B. Stefanov, G. Liu, A. Liashenko, P. Piskorz, I. Komaromi, R. L. Martin, D. J. Fox, T. Keith, M. A. Al-Laham, C. Y. Peng, A. Nanayakkara, M. Challacombe, P. M. W. Gill, B. G. Johnson, W. Chen, M. W. Wong, C. Gonzalez and J. A. Pople, *GAUSSIAN 03 (Revision B.01)*, Gaussian, Inc., Wallingford, CT, 2004.
47 J. Tomasi, B. Mennucci and R. Cammi, *Chem. Rev.*, 2005, **105**, 2999–3093.
48 H. Z. Malina, *Exp. Eye Res.*, 2004, **79**, 443–445.
49 R. W. Taft and M. J. Kamlet, *J. Am. Chem. Soc.*, 1976, **98**, 2886–2894.
50 M. J. Kamlet, J.-L. M. Abboud, M. H. Abraham and R. W. Taft, *J. Org. Chem.*, 1983, **48**, 2877–2887.
51 B. Lang, G. Angulo and E. Vauthey, *J. Phys. Chem. A*, 2006, **110**, 7028–7034.

52 A. Fürstenberg and E. Vauthey, *J. Phys. Chem. B*, 2007, **111**, 12610–12620.
53 W. Jarzeba, G. C. Walker, A. E. Johnson, M. A. Kahlow and P. F. Barbara, *J. Phys. Chem.*, 1988, **92**, 7039–7041.
54 R. Jimenez, G. R. Fleming, P. V. Kumar and M. Maroncelli, *Nature*, 1994, **369**, 471–473.
55 E. J. Hart and M. Anbar, *The Hydrated Electron*, Wiley-Interscience, New York, 1970, p. 42.
56 G. V. Buxton, C. L. Greenstock, W. P. Helman and A. B. Ross, *J. Phys. Ref. Data*, 1988, **17**, 513–886.
57 P. S. Sherin, J. Grilj, Yu. P. Tsentalovich and E. Vauthey, *J. Phys. Chem. B*, 2009, **113**, 4953–4962.